Journal of Alloys and Compounds 504 (2010) 32–36

Contents lists available at ScienceDirect

Journal of Alloys and Compounds

journal homepage: www.elsevier.com/locate/jallcom

TiO_x/N_y nanowire arrays: NH_3-assisted controllable vertical oriented growth and the electrophotochemical properties

Xin Wang [a], Yu Lin Yang [a,*], Ruiqing Fan [a,*], Yonghui Wang [b], Zhao Hua Jiang [a]

[a] Department of Chemistry, Harbin Institute of Technology, Harbin, 150001, PR China
[b] Key laboratory of Polyoxometalate Science of Ministry of Education, Faculty of Chemistry, Northeast Normal University, Changchun, 130024, PR China

ARTICLE INFO

Article history:
Received 24 March 2010
Received in revised form 28 April 2010
Accepted 5 May 2010
Available online 20 June 2010

Keywords:
Nanomaterials
Nanowires
Semiconductors
Chemical synthesis
Highly oriented growth
Electrophotochemical properties

ABSTRACT

In this research, a simple and facile approach was reported for the synthesis of highly oriented TiO_x/N_y nanowire arrays that originated from TiO_2 nanoparticles. The results indicated that nanowire arrays were fabricated with controllable lengths by adjusting the amount of NH_3 under medium pressures. The preferable orientation of nanowires was (1 0 3) crystal facet, which led to remarkable V_{oc} values in comparison with TiO_2 nanoparticles. An NH_3-assisted vapor–liquid–solid (VLS) growth mechanism was proposed for the direct growth of nanowire arrays from TiO_2 nanoparticles.

1. Introduction

Since Grätzel developed solar cells based on the nanocrystalline TiO_2 electrode [1], dye-sensitized solar cells (DSCs) have attracted much attention for their relatively low cost and high photoelectrical property [2–4]. A variety of methods have been devised to fabricate nanoscale TiO_2 film electrode to obtain high energy conversion efficiency for solar cells. Among the abundant reasonable designs, nitrogen-doped TiO_2 has shown prominent behavior since Ma et al. reported N-doped TiO_2 electrode could be used to improve the overall conversion efficiency (η) in 2005 [5]. However, the researchers have only paid attention to the nanoparticle materials. One-dimensional nanowires (NWs) have excellent physical and chemical properties in the applications of nanoscale electronic and optical devices [6,7]. Moreover, oriented nanostructures have demonstrated many excellent properties for energy harvesting, conversion and storage owing to their fast electron transport and straight conduction pathways [8,9]. Nanowires generally have preferred growth directions; therefore the controlled synthesis of NWs with orientation growth is becoming more and more important. In recent years a variety of techniques have been reported on NW synthesis, such as chemical vapor deposition (CVD) [10], pulsed laser deposition (PLD) [11,12], chemical beam epitaxy (CBE) [13], microwave plasma [14], evaporation [15], electrochemical deposition [16], e-beam lithography (EBL) [17], and thermal decomposition in aqueous solution [18], etc. Generally speaking, traditional methods fabricate randomly oriented NW arrays on the substrate surface. Although the electrochemical deposition procedure can implement precise orientation control, its process is complicate and requires higher costs. Considering production costs and operational techniques for applications, developing a relatively simple and mild process for preparing highly oriented nanowire arrays seems necessary. In the present work, we report a simple and facile approach for the controllable synthesis of vertical oriented nanowire arrays with N atom doped originating from TiO_2 nanoparticles, which depends on adjusting the amount of NH_3 gas injected in the reaction. The possible growth mechanism of the as-synthesized oriented nanowires was proposed and their electrophotochemical properties were studied by assembling the nanowire photoelectrodes for solar cells.

2. Experimental

2.1. Materials

Titanium isopropoxide, LiI, *tert*-butyl pyridine, acetonitrile and propylene carbonate were purchased from Aldrich Chemical Company and the dye N719 was used as received from Solaronix Company.

* Corresponding authors. Tel.: +86 451 86413710; fax: +86 451 86418270.
E-mail addresses: ylyang@hit.edu.cn (Y.L. Yang), fanruiqing@hit.edu.cn (R. Fan).

0925-8388/$ – see front matter © 2010 Elsevier B.V. All rights reserved.
doi:10.1016/j.jallcom.2010.05.053

2.2. Preparation

Nanocrystalline titania powder was synthesized by a hydrothermal method with titanium isopropoxide used as titanium source. Highly oriented nanowire films were prepared by a two-step process. Firstly, the raw TiO_2 films were prepared on F-doped SnO_2-coated (FTO) substrates by a screen-printed method using nanocrystalline titania powder and gradually sintered at 450 °C in dry air for device fabrication. Secondly, the sintered films were put in a sealed stainless steel autoclave designed by ourselves (see Supporting information) and treated in NH_3 with pressures ranging from 0 to 0.8 MPa (0, 0.2, 0.6, and 0.8 MPa) at 400 °C for 12 h. The NH_3 gas with 99% purity was first purified via a device that absorbed impurities and then flowed into the reaction chamber. The heater power was not launched until the NH_3 pressure reached the predetermined value [19].

2.3. Characterization

The phase structures of the raw and NH_3-treated films were characterized by powder X-ray diffraction (JDX-3530 M, Japan) using Ni filtered Cu Kα radiation. The X-ray photoelectron spectra were obtained in ultra-high-vacuum (UHV) at 3.5×10^{-7} Pa generated by a Thermo ESCALAB-250 spectrometer equipped with an Al Kα source. The surface morphologies of the raw and processed films were observed using a scanning electron microscope (SEM S-IRION, American-FEI Company; Hitachi S-4800). Crystallite sizes and shapes were observed using high-resolution transmission electron microscopy (HR-TEM) examination, which was conducted employing a JEM-2010 microscope (JEOL, 2100F, Japan) working at 200 kV.

2.4. Photoelectrochemical measurements

Each sample was sandwiched between two optically transparent (90% transmittance in the visible region), FTO glass electrodes (15 Ω^{-1} per square) which were purchased from Geao Equipment Company, Wu Han. The electrolytes used in this work were a mixture of 0.5 M LiI + 0.05 M I_2 + 0.1 M *tert*-butyl pyridine in 1:1 (volume ratio) acetonitrile–propylene carbonate. The films were stained by immersing in a 3×10^{-4} M solution of N719 in absolute ethanol for about 12 h. Photovoltaic performances were measured by using a mask with an aperture area of 0.238 cm^2 and the irradiance of sunlight was 100 mW cm^{-2}.

Based on the *J–V* curve, the fill factor (FF) is defined as

$$FF = \frac{J_{max} \times V_{max}}{J_{sc} \times V_{oc}}$$

where J_{max} and V_{max} are the photocurrent density and photovoltage for maximum power output (J_{sc} and V_{oc} are the short-circuit photocurrent density and open-circuit photovoltage, respectively.) And η is defined as the overall energy conversion efficiency, namely $\eta = (FF \times J_{sc} \times V_{oc})/P_{in}$, where P_{in} is the power of incident light.

3. Results and discussion

3.1. XRD patterns

Fig. 1 shows the XRD patterns of TiO_2 films before and after NH_3 gas treatment, indicating the phase-structural evolution of TiO_2 films induced by NH_3 injection. The present patterns both show some peaks (crystal face indexes: 1 0 1, 1 0 3, 2 0 0 and 1 0 5) characteristic of anatase TiO_2 and others (marked by the dark blue dots) originating from SnO_2 coated on the substrates. This fact confirms that both the raw and processed TiO_2 films essentially possess the phase structure of anatase TiO_2. Nevertheless, it is worth noting that the NH_3-treated films exhibit relative ascending diffraction at 37.9° in contrast with the raw TiO_2 films. This diffraction is consistent with the (1 0 3) inter planar spacing and may derive from the well-aligned nanowires vertically grown along (1 0 3) facets on the FTO glass. Such a preferable orientation can be attributed to the restrained oriented growth on a certain crystal facet. The possible growth mechanism will be discussed in the following sections.

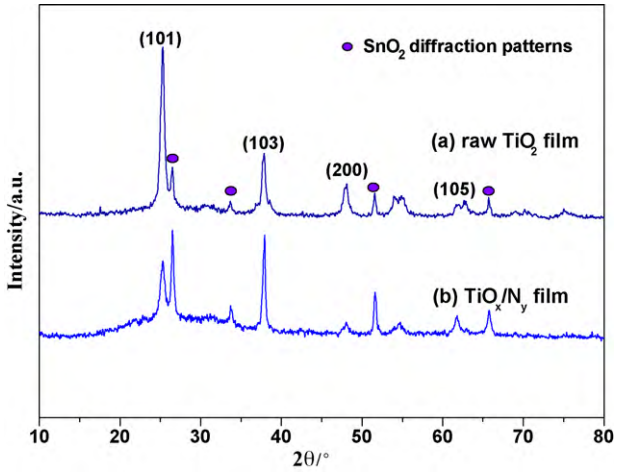

Fig. 1. XRD patterns of (a) raw TiO_2 films; (b) TiO_2 films treated under 0.6 MPa of NH_3 at 400 °C for 12 h (JCPDS No. 01-0562).

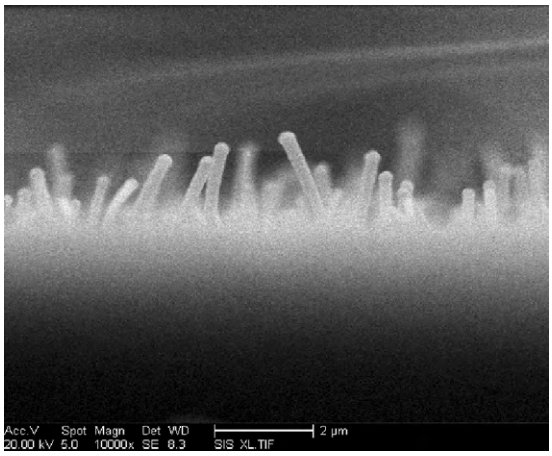

Fig. 2. The SEM image of the TiO_x/N_y nanowire arrays synthesized in NH_3 (0.6 MPa) at 400 °C for 12 h.

3.2. SEM and HR-TEM characterization

Based on earlier studies, the average grain size is approximate 10 up to 50 nm before thermal treatment in NH_3 atmosphere. Obviously, the raw TiO_2 films did not result in TiO_x/N_y nanowires [19].

Fig. 2 displays the SEM image of nanowire arrays synthesized via NH_3 (0.6 MPa) treatment at 400 °C for 12 h. As shown, the nanowires were coral-like with an average length of approximate 1.8 μm and highly oriented. This morphology suggests that surface reconstruction must occur during the NH_3 treatment and favor oriented growth of nanowires on the (1 0 3) facet. Further, in order to investigate the effects of the NH_3 amount on the morphology of nanowires, a series of experiments were carried out with different NH_3 pressures (0.2 and 0.8 MPa). The SEM results indicate that the nanowire length increased with enhancing the NH_3 concentration (Table 1). The nanowires synthesized in with the lowest NH_3 pressure of 0.2 MPa are short with an average length of only ca. 0.9 μm (see Fig. 3), whereas those obtained with 0.8 MPa of NH_3 are extremely long (ca. 3 μm). The possible growth process of nanowires can be explained as follows.

Upon heating, the TiO_2 precursors in the layers began to segregate and diffused to the surface to form TiO_2 droplets. These droplets were then reduced by NH_3 in the sealed device to form TiO_x/N_y. The generation rate of TiO_x/N_y was much faster than the diffusion rate of TiO_2 since formation of Ti–N–O transition state generally goes fast kinetics. This Ti–N–O species existed as solid particles and acted as nuclei that triggered further growth of the

Table 1
The average length of nanowires synthesized under different pressures of NH_3.

NH_3 pressure in system (MPa)	0	0.2	0.6	0.8
Average length of nanowires (μm)	–	0.9	1.8	3.0

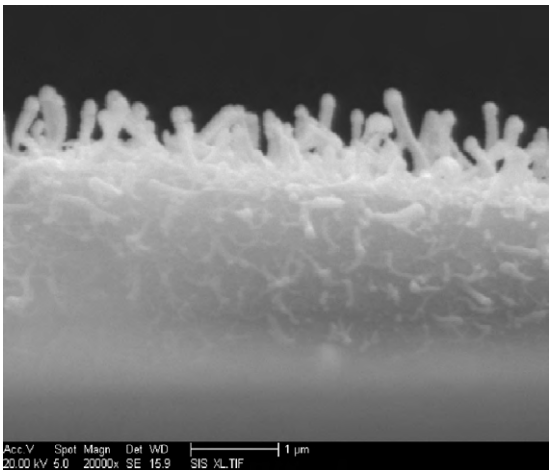

Fig. 3. The SEM image of the TiO_x/N_y nanowire arrays synthesized in NH_3 (0.2 MPa) at 400 °C for 12 h.

TiO_x/N_y nanowires. The growth of nanowires continued as long as TiO_x/N_y diffused from the layer to the tip. When the nanowires reached a certain length, the TiO_x/N_y diffusion became less efficient and the growth slowed down. Therefore, a conclusion can be drawn that the axial growth rate of nanowires increased with increasing the NH_3 concentration and taller nanowires tended to bend readily. The occurrence of tapering during the nanowire growth under relatively high NH_3 pressure (0.8 MPa) was highly detrimental to electron transfer. In a word, the use of NH_3 with a relatively high pressure retained the droplets on the tip via suppressing their diffusion, resulting in changes in the length of NWs.

High-resolution transmission electron microscopy images of TiO_x/N_y nanowires are provided in Fig. 4. An overview of the NWs at low magnification in SEM shows that the sample almost exclusively contains nanowires with an average length of 2 μm and diameters of approximately 20 nm. The single-crystalline nature of the NWs, with perfect an anatase structure, is clearly visible. The fringe spacing parallel to the main axis of the nanowires is estimated to be 0.357 nm, which is close to the (1 0 3) lattice spacing (0.343 nm) of anatase TiO_2. It indicates that crystal growth is preferential in the (1 0 3) direction, which results in isotropic growth of the nanocrystals, leading to elongated nanowires.

Furthermore, in order to eliminate the doubt whether other gases can also induce the formation of TiO_2 NWs, a control experiment using N_2 instead of NH_3 was performed. The result indicates that N_2 treatment of the raw TiO_2 films did not result in TiO_x/N_y nanowires. Therefore, this result supplies another proof for the NH_3-assisted growth mechanism of nanowires we have proposed (vide infra).

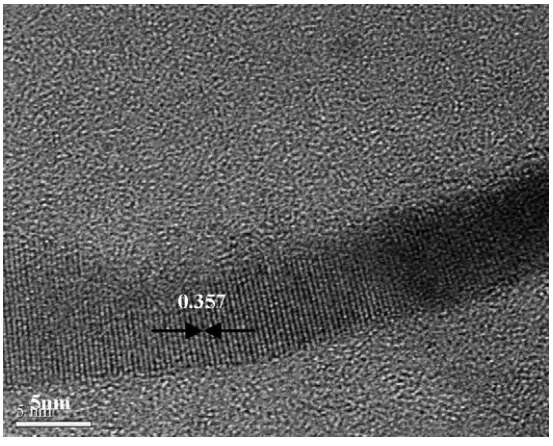

Fig. 4. HR-TEM images of the anatase TiO_x/N_y nanowires.

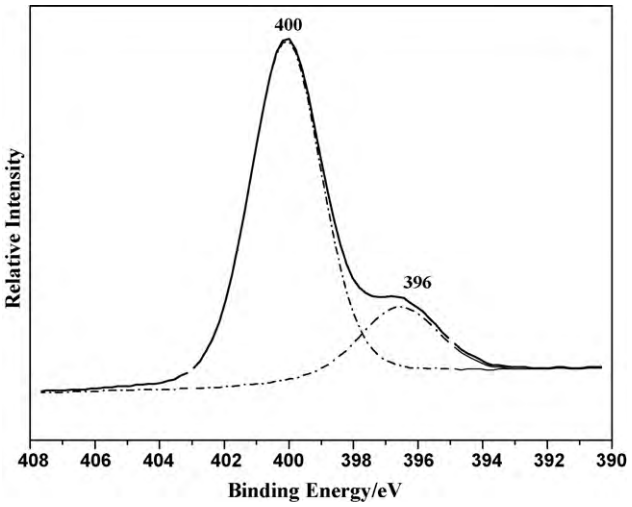

Fig. 5. The XPS spectrum of N 1s core-level of NW films synthesized in NH_3 (0.6 MPa) at 400 °C for 12 h.

3.3. XPS analysis

As shown in Fig. 5, the XPS spectrum of the nanowire films shows two differential peaks of N 1s centered at 396 and 400 eV, respectively [20]. The 400 eV band can be attributed to molecularly chemisorbed dinitrogen γ-N_2. The 396 eV peak is assigned to atomic β-N bonded to Ti, i.e. the atomic N sites that replaced O in the reaction.

3.4. SPS analysis

The surface photovoltage spectrum (SPS) method is commonly applied to TiO_2 for dye-sensitized solar cells, which is a well established contactless technique for surface state distribution. As shown in Fig. 6, the SPS analysis is described for samples with TiO_x/N_y NWs and raw TiO_2 photoelectrodes. It demonstrates that one typical characteristic response band close to 350 nm, which originates from the band–band electron transition of TiO_2, is observed. However, for NWs photoelectrode, a new SPS signal from 500 to 700 nm is observed, assigns to the band–band electron

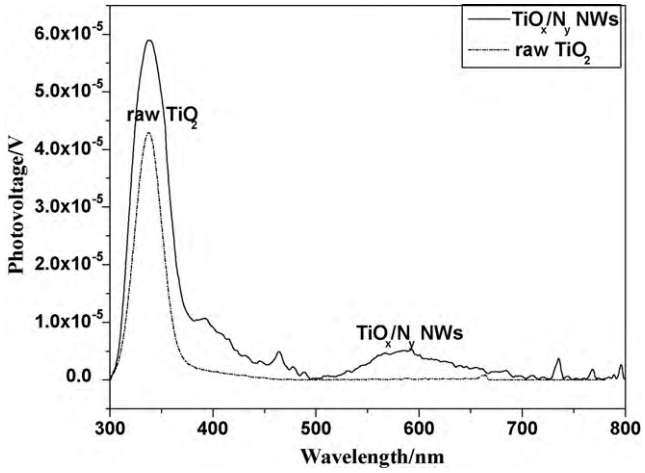

Fig. 6. SPS spectrum of raw TiO_2 and TiO_x/N_y NWs samples.

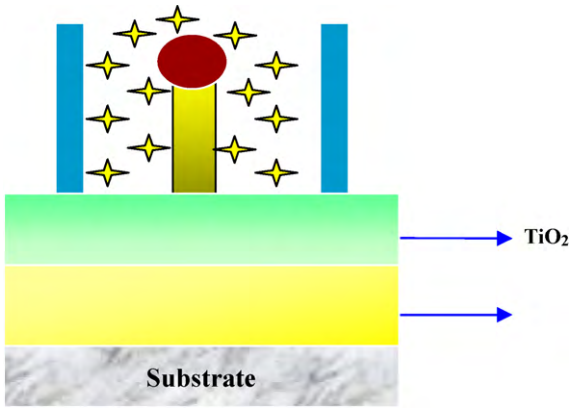

Fig. 7. Schematic view of the growth of the TiO_x/N_y nanowires.

transition of the N-doped band in NWs. The results also show that the TiO_x/N_y NWs are benefit for the visible light response range broadened that ranged from 400 to 700 nm.

3.5. Mechanism

Effective applications can only be realized if the nanostructures are self-assembled, which requires a clear understanding of the growth mechanism [21–23]. The first growth mechanism of wire-like morphology in metallic and ceramic systems was proposed several decades ago [24]. However, the structures and defects have not been totally understood yet and the growth mechanism remains debated.

Based on the mechanisms of crystal growth, we propose a possible growth mechanism for the transformation of TiO_2 from nanoparticles to 1D NWs, namely the NH_3-assisted VLS (vapor–liquid–solid) process (see Fig. 7). What is crucial to this growth mechanism is that the reaction of TiO_2 and NH_3 leads to the formation of TiO_x/N_y transitional state. In the reaction, NH_3 acts as a kind of reductant (Eq. (1))

$$NH_3 + TiO_2 \rightarrow \left(\frac{TiO_x}{N_y}\right) + H_2O \quad (1)$$

In our experiments, particles were observed on the top of the nanowires that directly grew from the layers. The precipitation, nucleation and growth of nanowires always occurred at the area near the cold finger, which suggests that the temperature gradient provided the external driving force for nanowire formation and growth [25,26]. By separately considering the nucleation and growth steps, we explain the morphology of NWs with the following model. Some TiO_x/N_y nanoparticles piled up on the matrix surface, which can act as crystal nuclei prevented the nanoparticles from congregating into micro-scale particles in a short time. It has been widely recognized that the surface melting temperature of nanoparticles can be much lower than that of their bulk materials [27,28]. When the dispersed nanoparticle reached their molten states before their agglomerate compound, TiO_x/N_y nanoparticles from the substrate would diffuse along the nanowire sidewalls towards their growing tips and contribute to axial growth. The main defects in nanowires were stacking along the nanowire growth direction of (1 0 3). The presence of these defects at the tip areas should result in the fast growth of nanowires. Consequently, it was believed that the nanowire growth described here was governed by an NH_3-assisted VLS growth mechanism since NH_3 doped into the lattice led to interior defects in the process of crystal growth [29,30,21,31]. The TiO_x/N_y crystal nuclei in the layers acted as a reactant and a catalyst simultaneously and diffused through the nanowires to the tip to maintain the growth.

Table 2
Comparison of *J–V* performances between nanowires treated by NH_3 and TiO_2 nanoparticles without treatment as photoelectrodes.

	Pressure (MPa)	V_{oc} (mV)	J_{sc} (mA cm^{-2})	FF	η (%)
Nanowires (NH_3)	0.8	542	2.60	0.27	1.14
	0.6	636	4.63	0.34	2.61
	0.2	748	1.82	0.62	2.84
Nanoparticles (N_2)		417	1.33	0.53	0.88

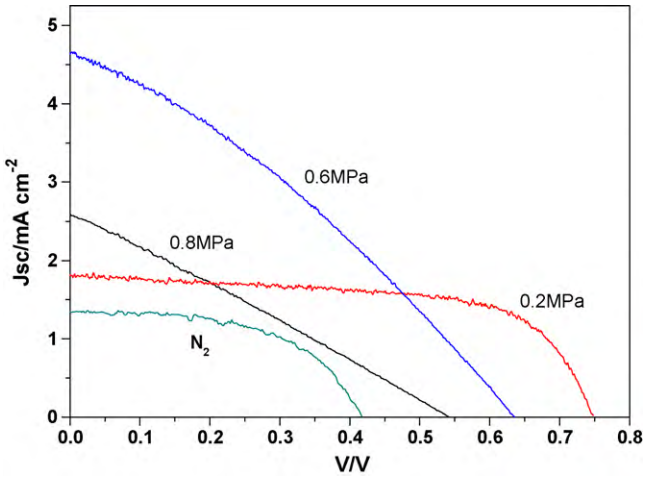

Fig. 8. *J–V* (current density–voltage) curves of the sunlight-illuminated dye-sensitized solar cells using nanowires synthesized under different NH_3 pressures (0.2, 0.6 and 0.8 MPa) and N_2 treatment as photoelectrodes.

3.6. Photoelectrochemical properties

Table 2 compares the performances of TiO_x/N_y nanowires and TiO_2 nanoparticles (synthesized in an atmosphere of N_2) as photoelectrodes. Interestingly, the V_{oc} of the photoelectrodes increased with the structure changing from nanoparticle to nanowire. In particular, the NWs photoelectrode synthesized under 0.6 MPa of NH_3 exhibited a remarkable V_{oc} in solar cells (see Fig. 8). However, the results also reveal that the η values of NWs enhanced with decreasing NH_3 pressure. Thus as photoelectrodes NWs were relatively inferior to nanoparticles in terms of FF. The reason lies in their structure and property, namely NWs had higher surface area/volume ratios and less agglomerated configuration. Therefore, the nanoscale structure with fewer amounts has a disadvantage of filling with electrolyte. However, the energy convert efficiency for nanowire structures is higher than the nanoparticle structures. Therefore, it can be safely concluded that highly oriented nanowire structures with high surface area/volume ratios and straight conduction pathways are advantageous to accomplish rapid electron transfer, which can reduce the recombination between injected carriers and holes in photoelectrodes. The current synthetic method can be potentially extended to produce NWs photoelectrodes for photoelectrochemical applications.

4. Conclusions

We have demonstrated a simple and facile approach for directly synthesizing highly oriented nanowire arrays from TiO_2 nanoparticles. Fine and dense NWs with a preferable growth orientation towards the (1 0 3) crystal facet were obtained by means of this method. The pressure of NH_3 had a major impact on the length of NWs via enhancing the longitudinal growth rate. Therefore, the length of the nanowires can be well controlled by varying the NH_3 pressure in the working environments. Moreover, we have

proposed an NH_3-assisted VLS growth mechanism to explain the growth of NWs. The present work provides a facile and promising process for synthesis of other single-crystalline metal oxides and large-area production of nanowires on substrates. And the current controllable synthetic method is expected to play an important role in the fabrication of electronic and optoelectronic devices in future.

Acknowledgments

This work was supported by the National Science Foundation of China (grant nos. 20971031, 20671025 and 20771030), the China Postdoctoral Science Foundation funded project (no. 65204).

Appendix A. Supplementary data

Supplementary data associated with this article can be found, in the online version, at doi:10.1016/j.jallcom.2010.05.053.

References

[1] B. O'Regan, M. Grätzel, Nature 353 (1991) 737.
[2] G.M. Lowman, P.T. Hammond, Small 1 (2005) 1070.
[3] N. Ikeda, T. Miyasaka, Chem. Commun. 5 (2005) 1886.
[4] Z.S. Wang, C.H. Huang, Y.Y. Huang, Y.J. Hou, P.H. Xie, B.W. Zhang, H.M. Cheng, Chem. Mater. 13 (2001) 678.
[5] T. Ma, M. Akiyama, E. Abe, I. Imai, Nano Lett. 5 (2005) 2543.
[6] J. Yang, J. Zheng, H. Zhai, X. Yang, L. Yang, Y. Liu, J. Lang, M. Gao, J. Alloys Compd. 489 (2010) 51.
[7] M. Law, L.E. Greene, J.C. Johnson, Nat. Mater. 4 (2005) 455.
[8] A. Ghicov, J.M. Macak, H. Tsuchiya, J. Kunze, V. Haeublein, S. Kleber, P. Schmuki, Chem. Phys. Lett. 419 (2006) 426.
[9] C.G. Granqvist, Sol. Energy Mater. Sol. Cells 91 (2007) 1529.
[10] R.S. Wagner, W.C. Ellis, Appl. Phys. Lett. 4 (1964) 89.
[11] A.M. Morales, C.M. Lieber, Science 279 (1998) 208.
[12] M.S. Gudiksen, L.J. Lauhon, J. Wang, D.C. Smith, C.M. Lieber, Nature 415 (2002) 617.
[13] B. Liu, S.A. Eray, J. Am. Chem. Soc. 131 (2009) 3985.
[14] C. Thelander, P. Agarwal, S. Brongersma, J. Eymery, L.F. Feiner, A. Forchel, M. Scheffler, W. Riess, B.J. Ohlsson, U. Gösele, L. Samuelson, Mater. Today 9 (2006) 28.
[15] M.H. Huang, S. Mao, H. Feick, H. Yan, Y. Wu, H. Kind, E. Weber, R. Russo, P. Yang, Science 292 (2001) 1897.
[16] E.J. Menke, Q. Li, R.M. Penner, Nano Lett. 4 (2004) 2009.
[17] H.T. Ng, J. Han, T. Yamada, P. Nguyen, Y.P. Chen, M. Meyyappan, Nano Lett. 4 (2004) 1247.
[18] W. Lu, C.M. Lieber, J. Phys. D 39 (2006) R387.
[19] X. Wang, Y. Yang, Z. Jiang, R. Fan, Eur. J. Inorg. Chem. (2009) 3481.
[20] H. Irie, Y. Watanabe, K. Hashimoto, J. Phys. Chem. B 107 (2003) 5483.
[21] H.J. Fan, P. Werner, M. Zacharias, Small 2 (2006) 700.
[22] S.C. Lyu, Y. Zhang, L.C.J. Ruh, H.J. Lee, Chem. Mater. 15 (2003) 3294.
[23] M. Salavati-Niasari, M.R. Loghman-Estarki, F. Davar, Chem. Eng. J. 145 (2008) 346.
[24] J.G. Wen, J.Y. Lao, D.Z. Wang, Chem. Phys. Lett. 372 (2003) 717.
[25] C.Y. He, X.Z. Wang, Q. Wu, Z. Hu, Y.W. Ma, J.J. Fu, Y. Chen, J. Am. Chem. Soc. 132 (2010) 4843.
[26] Y.C. Kong, D.P. Yu, B. Zhang, Appl. Phys. Lett. 78 (2001) 407.
[27] V. Schmidt, S. Senz, U. Gosele, Nano Lett. 5 (2005) 931.
[28] Z.W. Pan, Z.R. Dai, C. Ma, Z.L. Wang, J. Am. Chem. Soc. 124 (2002) 1817.
[29] A.C. Gandhi, H.J. Hung, P.H. Shih, C.L. Cheng, Y.R. Ma, S.Y. Wu, Nanoscale Res. Lett. 5 (2010) 581.
[30] Y.L. Chiew, K.Y. Cheong, Phys. E: Low-Dimensional Syst. Nanostruct. 42 (2010) 1338.
[31] R.P. Vitiello, J.M. Macak, A. Ghicov, H. Tsuchiya, L.F.P. Dick, P. Schmuki, Electrochem. Commun. 8 (2006) 544.